applied sciences

MDPI

Article

Assessment of the Effects of Temperature and CO_2 on Methane Leak Detection and Quantification Using Optical Gas Imaging Technologies

Abir Kebir, Hossein Emadi * and Jemal W. Fentaw

Bob L. Herd Department of Petroleum Engineering, Texas Tech University, Lubbock, TX 79409, USA; akebir@ttu.edu (A.K.); jfentaw@ttu.edu (J.W.F.)

* Correspondence: h.emadibaladehi@ttu.edu

Abstract

Assessing methane (CH_4) emissions is critical for mitigating the environmental impact of greenhouse gases (GHGs). Optical Gas Imaging (OGI) technologies have emerged as effective tools for gas leak detection and quantification; however, their performance under varying environmental conditions and gas compositions remains insufficiently understood. In particular, previous studies have largely overlooked the combined effects of ambient temperature variations and Carbone. Dioxide (CO_2) interference on both detection sensitivity and quantification accuracy. This study addresses this gap by systematically investigating the influence of temperature and CO_2 on methane detection and quantification using an infrared OGI camera coupled with real-time analysis software. Logistic regression was employed to model detection probability under two temperature conditions at a fixed distance of 45 m. Results show that at 30 °C, the system achieved 50% and 90% detection probabilities at 5.51 and 11.30 kg/h, respectively. In contrast, at −7 °C, detection reliability decreased due to increased false positives, preventing the establishment of robust detection thresholds. However, methane quantification accuracy improved under colder conditions, with 90% of leaks correctly quantified compared to 60% in warmer environments. Furthermore, the presence of CO_2 completely inhibited methane detection and quantification. These findings demonstrate the significant and previously underexplored impact of temperature and gas composition on OGI performance, highlighting critical limitations in real-world applications and providing new insights for improving methane monitoring strategies.

Keywords: methane; detection and quantification; optical gas imaging; logistic regression

Check for updates

Academic Editor: Arcady Dyskin

Received: 27 March 2026
Revised: 17 May 2026
Accepted: 20 May 2026
Published: 26 May 2026

Copyright: © 2026 by the authors. Licensee MDPI, Basel, Switzerland. This article is an open access article distributed under the terms and conditions of the Creative Commons Attribution (CC BY) license.

1. Introduction

Global warming is one of the most significant global environmental problems at present. The increased dependence on fossil energy resources and large-scale deforestation have led to an increase in anthropogenic greenhouse gases, which are one of the reasons for global warming [1]. The primary greenhouse gases and their relative proportions include water vapor, H_2O (g) (36–70%), carbon dioxide, CO_2 (9–26%), methane, CH_4 (4–9%), nitrous oxide, N_2O (3–7%), in addition to several trace gases. Among these, CO_2 and CH_4 are commonly known as key contributors to the increase in global surface temperatures due to their growing concentrations and high global warming potential [2]. Particularly, methane affects temperatures directly through radiation absorption and indirectly through

chemical reactions. Methane influences the abundance of ozone in the troposphere and the stratosphere, resulting in stratospheric water [3]. Unless prominent mitigation measures are executed, additional increases are anticipated. This brings into sharp focus the new strategies that need to be employed in combating greenhouse gas emissions, including switching over to renewable energy sources, promoting the use of carbon capture technologies, and enhancing methane emissions monitoring and reduction systems [4–6].

Methane, in particular, plays a dual role in climate dynamics. It directly contributes to warming through its absorption of infrared radiation and indirectly influences atmospheric chemistry, including the formation and destruction of ozone in the troposphere and stratosphere, which subsequently affects stratospheric water vapor concentrations [5]. Studies estimate that methane has a 20-year Global Warming Potential (GWP) of approximately 84–86 times that of CO_2, emphasizing its importance for near-term climate mitigation. Reducing methane emissions could slow the rate of warming by up to 0.3 °C over the next two decades, according to recent climate studies [6,7]. The Intergovernmental Panel on Climate Change (IPCC) reports that anthropogenic activities have already caused approximately 1.5 °C of global warming above pre-industrial levels, with further increases likely unless robust mitigation measures are implemented [8]. Strategies to reduce GHG emissions, therefore, include transitioning to renewable energy sources, deploying carbon capture and storage (CCS) technologies, improving energy efficiency, and enhancing methane monitoring and abatement systems [9,10].

Optical gas imaging is a non-contact technique widely employed for detecting gaseous emissions, particularly methane and volatile organic compounds (VOCs), in industrial and environmental contexts. OGI systems use thermal infrared cameras to visualize invisible gases by detecting differences in thermal radiation between gas plumes and their surroundings. This enables the rapid identification of leaks and supports the reduction in fugitive emissions in oil and gas operations, waste management facilities, and chemical plants [11–14].

Despite its advantages, OGI technology exhibits limitations. Detection sensitivity and quantification accuracy are influenced by ambient temperature, wind speed, background thermal conditions, gas composition, and optical path length [15,16]. Among these, ambient temperature and thermal contrast are particularly critical because OGI relies on differential radiative signatures; insufficient thermal contrast can result in false negatives or underestimation of emissions [17]. In this study, we did not implement the wind speed and the humidity as variables because their variations were not significant. The only variable that we could control its variation was methane flow rate.

Previous studies have investigated OGI performance under varying environmental conditions. For instance, Smith et al. [18] reported that the detection probability for a 0.2 kg/h methane leak ranged from 50% to 85% at 0 °C to 25 °C. These results underscore the necessity of understanding environmental influences when deploying OGI systems for regulatory compliance and emissions reporting. A summary of select studies examining the effect of ambient temperature on OGI detection performance is presented in Table 1.

These findings highlight that both detection probability and quantification accuracy are highly sensitive to ambient conditions, particularly temperature and thermal contrast. However, few studies have systematically explored the relationship between nature conditions, detection probability, and quantification accuracy under controlled leak scenarios [19–21]. While previous studies have investigated methane detection using Optical Gas Imaging under controlled conditions, limited attention has been given to the combined effects of ambient temperature variations and CO_2 interference on detection sensitivity and quantification accuracy.

Table 1. Summary of Reported OGI Methane Detection Probabilities and Quantification Errors Under Varying Ambient Temperatures.

Study	Gas	Leak Rate	Ambient Temperature	Detection Probability	Quantification Error
Zimmerle et al., 2015 [17]	CH_4	1 kg/h	30 °C	70%	±35%
Smith et al., 2020 [18]	CH_4	0.2 kg/h	0–25 °C	50–85%	±20–30%

In this study, we aim to fill this gap by evaluating the performance of an infrared camera system for real-time detection and quantification of methane under varying ambient temperatures (30 °C to −7 °C), with a focus on determining its precision and accuracy. The experiments focus on how thermal contrast affects the reliability of OGI measurements. By providing a more quantitative understanding of these relationships, this research contributes to improving the accuracy of methane emissions reporting and the design of effective leak mitigation strategies, which are crucial for advancing climate change mitigation efforts.

2. Infrared Thermal Imager and Imaging Properties

Infrared (IR) radiation is a form of electromagnetic energy that results from quantum transitions between discrete energy levels in atoms or molecules. These transitions are associated with the rotational and vibrational modes of molecular bonds, particularly in gases. According to Planck's law of blackbody radiation, any object with a temperature above absolute zero (0 K) emits electromagnetic radiation, with intensity and wavelength characteristics that depend on its temperature. As temperature increases, both the intensity and the peak wavelength of emitted radiation shift, with hotter objects emitting more strongly at shorter infrared wavelengths—a principle exploited in thermal imaging systems [22–25].

Thermal infrared imaging typically operates within the mid-infrared (MIR, ~3–5 μm) and far-infrared (FIR, ~8–14 μm) spectral bands. These regions correspond to atmospheric transmission windows where absorption by air components is minimized, allowing IR cameras to effectively observe radiation emitted or absorbed by gases such as methane [26].

Methane exhibits distinct absorption features at specific infrared wavelengths due to vibrational transitions. These are primarily found at approximately 3.3–3.5 μm and 7.6–8 μm, making these regions optimal for detecting CH_4 using infrared sensors. These narrow absorption bands form what is referred to as a spectral fingerprint, allowing for the selective identification of methane among other gases. Additionally, wavelengths between 2200 nm and 2400 nm (2.2–2.4 μm) are also absorbed by CH_4 in a unique pattern, making tunable diode laser absorption spectroscopy (TDLAS) and narrowband infrared cameras effective tools for high-sensitivity methane detection [27–29].

The molecular structure and mass of the gas have a significant impact on its absorption spectrum. Specifically, the atomic and molecular weights of methane determine how it interacts with IR radiation through vibrational and rotational modes [30]. The vibrational frequency (ν) of a diatomic molecule, modeled as a simple harmonic oscillator, is given by the following equation:

$$\nu = 130.3 \sqrt[2]{\left(f \left[\frac{1}{m_1} + \frac{1}{m_2} \right] \right)} \quad (1)$$

where f is the bond force constant (Nm^{-1}), and m_1 and m_2 are the masses of the atoms 1 and 2, respectively.

This equation helps predict the vibrational transition frequencies, which determine the spectral location of absorption lines in gases like methane.

When methane forms a homogeneous medium, such as in a gas plume, its interaction with infrared radiation is governed by the Beer-Bouguer-Lambert Law (shown in Equation (2) below), which quantifies how much radiation is absorbed as it passes through an absorbing medium:

$$I = I_0 e^{-\mu d} \quad (2)$$

where I_0 is the initial intensity of the light, I is the intensity of the light after travelling the distance d in the medium, and μ is the Napierian absorption coefficient often called the optical density.

This exponential relationship underpins the optical detection of gas concentrations, with higher gas densities and longer path lengths resulting in greater signal attenuation. For large methane plumes, higher concentrations lead to stronger absorption, resulting in more intense infrared signals and easier detection [31–33].

Optical gas sensors, including thermal IR cameras, work by detecting the changes in radiance caused by gas plumes absorbing IR radiation. These sensors capture variations in electromagnetic energy, which correspond to molecular vibrations and transitions. In particular, uncooled infrared cameras—like the one used in this study—are designed to operate efficiently in the atmospheric windows where CH_4 absorbs and emits radiation most clearly [34].

The application of the Beer–Bouguer–Lambert law in OGI-based methane quantification assumes a homogeneous gas distribution and a well-defined optical path length. However, under field conditions with variable wind, the methane plume becomes highly heterogeneous and turbulent, resulting in spatial and temporal fluctuations in concentration. Consequently, the measured attenuation represents a path-integrated quantity rather than a local concentration, introducing ambiguity in quantification. These effects are further exacerbated by plume intermittency and mixing with other gases such as CO_2, which alter the effective absorption characteristics. As a result, deviations from ideal Beer–Lambert behavior contribute to increased uncertainty and reduced accuracy in methane quantification.

3. Leak Modeling and Experimental Setup

In this study, methane plumes were generated under controlled conditions to model realistic leak scenarios from various sources, including natural gas wells, unplugged or abandoned wells, pipeline leaks, and oil and gas processing facilities. These simulated plumes provided a testbed for assessing the camera's performance in real-world leak detection, with controlled variation in leak rates, ambient environmental conditions, and viewing geometry.

By understanding the underlying physical principles of infrared radiation and the specific absorption behavior of methane, the IR camera system could be calibrated and optimized for improved detection sensitivity. The spectral fingerprint of methane, combined with advanced image processing algorithms and machine learning models, enables the development of robust gas leak detection frameworks that inform regulatory compliance, environmental monitoring, and pipeline integrity programs [35,36].

To evaluate the performance of an Optical Gas Imaging system in detecting and quantifying methane emissions, a controlled leak experiment was conducted at the Oil Technology Center, Texas Tech University, in Lubbock, TX. The experiment was carefully designed to simulate realistic field leak scenarios under varying environmental conditions while allowing for precise control and measurement of gas flow rates.

Methane was released from pressurized bottles ranging from 500 to 2200 psia, supplying gas to a custom-built mobile emitter. The emitter was constructed using a ¾-inch diameter pipe (Figure 1a), securely connected to the methane supply (Figure 1b).



(a) (b)

Figure 1. (**a**): 3/4″ Mobile Emitter. (**b**): Metering Station.

The methane bottles were connected to a manifold system that included:

- Three manual valves for isolating and controlling gas flow paths;
- A high-precision pressure regulator to ensure consistent outlet pressure;
- Pressure gauges to monitor upstream and downstream pressures;
- A high-accuracy mass flow meter, and
- A flow control valve for adjusting and fine-tuning the methane emission rate.

The entire gas handling system was monitored and controlled through Flow Vision 2.0 software, which logged real-time flow rate and operational data. The metering station was connected at one end to the methane emitter and at the other to the software interface, allowing for continuous monitoring and precise control of emission parameters.

Methane emissions were visualized and recorded using a fixed, uncooled infrared (IR) camera, positioned at a fixed distance of 45 m from the mobile emitter. This camera is equipped with a 640 × 480-pixel focal plane array (FPA) and a 17 µm pixel pitch, enabling high-resolution thermal imaging. It operates at 25 frames per second (FPS), which allows for near real-time video capture of leak dynamics. The use of an uncooled IR sensor made the camera suitable for outdoor use, with minimal thermal lag and distortion, particularly in field conditions.

Throughout the study, no artificial wind sources (such as fans or blowers) were introduced. As a result, the dispersion and movement of methane plumes were dictated solely by natural wind conditions, providing realistic challenges for OGI performance under field-like circumstances. The ambient wind patterns significantly influenced the shape, direction, and stability of the plume—key factors in successful plume detection and quantification.

Over the course of the experiment, a total of 7278 measurement points were collected. These included observations made at different times of day and under varying temperature conditions. Before modeling, a data cleaning process was performed to enhance model robustness. This involved:

- Removing all data points with zero recorded methane flow (no leak condition) and

- Eliminating false positive detections, where a plume was identified but no leak was actually present, based on flow meter readings.

Post-cleaning, the dataset retained only True Positive (TP) and False Positive (FP) cases to ensure the model's accuracy in evaluating detection success rates under actual emission conditions.

Leak rates were modulated by ambient temperature:

- On warmer days, methane emission rates ranged from 4 to 7 kg/h and
- On colder days, release rates were lower, between 0 and 4 kg/h, as these conditions naturally reduced plume buoyancy and detection clarity.

3.1. Probabilistic Model: Logistic Regression for Detection Prediction

To analyze the detection efficiency of the IR camera as a function of methane emission rate, a logistic regression model was applied. This statistical model is particularly well suited for classification problems where the dependent variable is binary—in this case, whether a leak was detected (1) or not (0). Moreover, since detection probability is a continuous variable bounded between 0 and 1, logistic regression provides an appropriate method for estimating the likelihood of detection at different emission levels.

The general form of the logistic function is:

$$p(x) = \frac{1}{1 + e^{-(\beta_0 + \beta_1 x_1 + \beta_2 x_2 + \ldots)}} \quad (3)$$

For this experiment, only one explanatory variable—methane flow rate (x_1)—was considered initially, simplifying the equation to:

$$p(x) = \frac{1}{1 + e^{-(\beta_0 + \beta_1 x_1)}} \quad (4)$$

where p is the predicted probability of detection, x is an input value (Flowrate in kg/h), e is Euler's number (~2.718), β_0 is the intercept term and β_1 is a coefficient for the input x [37–39].

This logistic model was trained using the cleaned dataset of TP and FP observations. The output curve generated by the model provides a probability of detection (PoD) as a function of emission rate. This PoD curve is essential for:

- Establishing detection thresholds (e.g., leak rates at which the camera reaches 50% or 90% detection);
- Benchmarking the IR system's performance against regulatory standards;
- Predicting detection success under unknown field conditions and
- Guiding operational decisions in emissions monitoring programs.

Future iterations of the model may include additional predictor variables, such as ambient temperature, wind speed, humidity, and background clutter, which could further enhance the predictive accuracy and generalizability of the detection probability function.

3.2. Blind Test

The initial phase of the study involved conducting a blind test to objectively evaluate the efficiency and reliability of the infrared (IR) camera for detecting methane leaks. This preliminary test was critical in establishing baseline performance under controlled environmental conditions before proceeding with more complex scenarios. Throughout the duration of this test, meteorological parameters were maintained at relatively stable levels to minimize variability and isolate the influence of the camera's detection capabilities.

The average ambient temperature during the blind test was approximately 25 °C, which falls well within the camera's optimal operating temperature range of −10 °C to +50 °C. This ensured that the thermal sensors were functioning within their designed performance envelope, thereby avoiding any thermal drift or sensor degradation that could compromise detection accuracy. Additionally, wind speeds averaged 15 miles per hour (mph), and relative ambient humidity was maintained around 25%. These conditions are significant, as wind speed influences plume dispersion and direction, while relative humidity affects infrared absorption and image contrast. The probability curve shows real results. No average values were calculated.

Prior to deployment, the IR camera was stored in conditions that adhered to its manufacturer-recommended storage temperature range of −40 °C to +71 °C. The storage facility recorded ambient temperatures ranging from −11 °C to 45 °C, indicating that the equipment had been maintained in an environment that preserved its operational integrity and sensor calibration. Proper storage is particularly important for IR imaging devices, as prolonged exposure to extreme temperatures outside this range can lead to sensor misalignment, decreased sensitivity, or hardware damage.

The results of the blind test (Figure 2) were promising: the camera achieved a 90% probability of detection (PoD), indicating a high level of reliability in identifying methane leaks under the given conditions. This metric is commonly used in leak detection performance assessments, and reaching the 90% PoD threshold signifies that the system can detect 9 out of 10 actual leak events, which is typically considered acceptable for field applications, regulatory use, and validation of leak detection technologies.

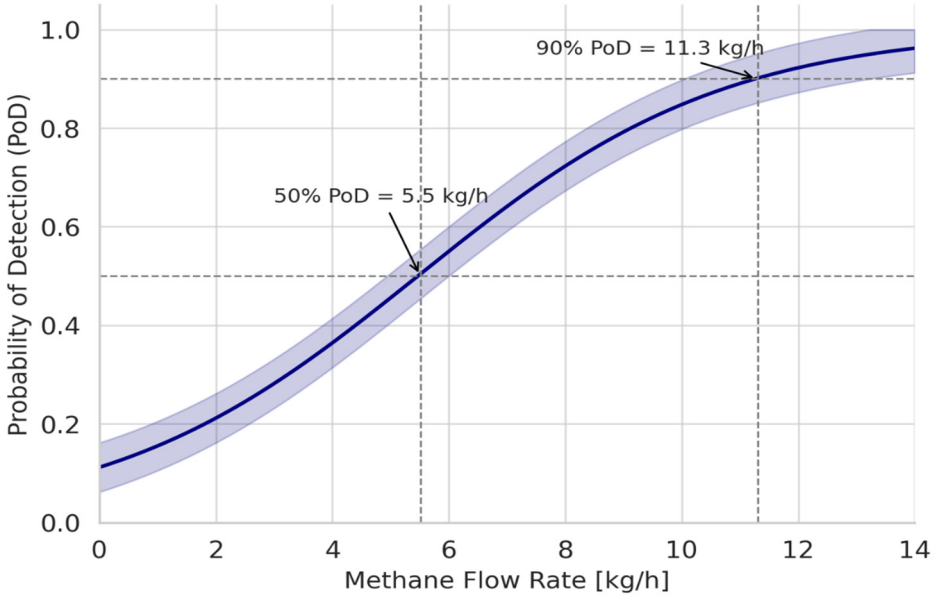


Figure 2. Probability curve of detection.

Given these favorable results, it was concluded that the IR camera was functioning as intended and could be confidently used in subsequent phases of the research. These follow-up experiments aimed to explore the camera's performance under colder environmental conditions. The successful completion of the blind test thus laid a solid foundation for more advanced evaluations of the camera's detection sensitivity, false positive rate, and quantification accuracy in real-world settings. The accuracy and precision are given by, respectively,

$$Accuracy = \frac{TP + TN}{TP + TN + FP + FN} \quad (5)$$

and

$$Precision = \frac{TP}{TP + FP} \quad (6)$$

where TP is True Positive, TN is True Negative, FP is False Positive, and FN is False Negative [39].

4. Results and Discussion

4.1. Detection and Quantification

A comparative analysis of the two experimental conditions, warm and cold ambient temperatures, reveals that methane leak detection using Optical Gas Imaging is considerably more effective on warmer days. During warm weather, the performance of the infrared (IR) camera significantly improves due to enhanced thermal contrast between the methane plume and the background, allowing for more accurate and consistent leak identification. Specifically, the IR camera achieved detection probabilities of 50% and 90% at methane leak rates of 5.51 kg/h and 11.30 kg/h, respectively. These detection thresholds indicate robust performance, where even moderately small leaks are reliably identified under higher ambient temperature conditions.

Conversely, under colder conditions, the detection efficiency dropped substantially. Attempts to develop a reliable predictive model for leak detection in the cold experiment were unsuccessful due to poor model convergence and low predictive power. These issues stemmed from increased variability in detection results and a significantly higher rate of false positives, which rendered statistical inference less meaningful. As a result, only descriptive statistics were reported for the cold weather conditions.

Interestingly, although detection performance was lower in the cold, the quantification of gas leak rates—i.e., the accuracy of estimating the amount of methane being emitted—was partially improved under colder conditions. This seemingly paradoxical result is attributable to the radiometric characteristics of the infrared imagery. The radiance contrast, which governs how visible the gas plume is in thermal imagery, is given by the equation:

$$\Delta L = B(T_s + \Delta T) - \epsilon_s B(T_s) \quad (7)$$

where $\Delta T = T_p - T_s$, T_p is the temperature of the gas plume, T_s is the ambient background temperature, ϵ_s is the emissivity of the background surface, and B(T) represents the Planck function describing blackbody radiation. In colder environments, the smaller value of T_s increases ΔT, thereby enhancing ΔL and making the plume more radiometrically distinguishable from the background. This leads to better estimation of gas volumes, even if detection itself is hindered.

Although colder environments increase the initial temperature contrast between the plume and the background, this advantage diminishes rapidly as the methane plume cools and equilibrates with the ambient air during dispersion. As a result, both the thermal contrast and absorption strength decrease with distance, leading to a reduction in radiance contrast which might increase false positives.

In summary, while warmer days favor better detection probabilities due to thermal contrast and visual clarity, colder conditions might sometimes offer more accurate quantification of emission rates due to higher radiance differentials. However, the trade-off lies in the increased false positive rate and inconsistent model behavior in colder settings, which limits their practical utility in real-time leak monitoring using OGI technologies.

Figure 3 illustrates the exact comparison of the actual methane release rate as the reference line, the Optical Gas Imaging measured rate, and the related gas temperature profile during the test, simultaneously measured.

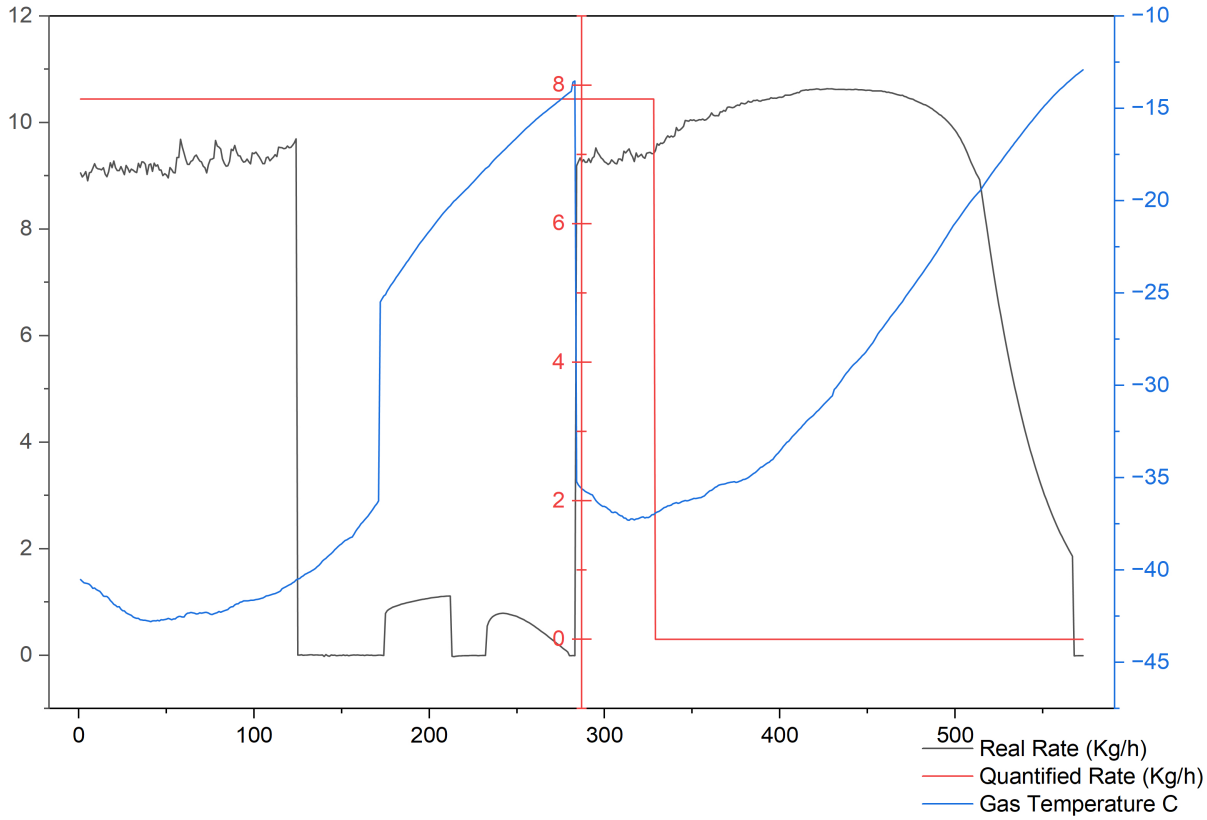


Figure 3. Rates of methane quantified by the OGI Camera.

It can be seen from the data that the OGI-quantified rate generally follows the size of the actual release but exhibits noticeable differences. During the early release phase, OGI underestimated the methane rate by approximately 1–2 kg/h, and it failed to account for sudden changes in the release profile. During subsequent phases, OGI quantification underestimated the emissions and showed periods of complete non-detection despite continued release. This inconsistency suggests that quantification of OGI is not sensitive to fluctuating emission rates and will overestimate or underestimate the actual size under certain operating conditions.

The gas temperature trace shows a steady increase from approximately –35 °C to approximately –5 °C during the experiment, followed by a subsequent steep decline. Such temperature variations are significant because OGI sensitivity is claimed to be a function of the thermal contrast between the gas plume and the ambient. Moments of OGI non-detection or underestimation are well correlated with instances of impaired thermal contrast, and it is most likely that temperature effects were the prime reasons behind impaired quantification performance.

In general, the comparison serves to illustrate the strengths and limitations of OGI as a measurement technology for detecting and quantifying methane. Although OGI successfully identified the existence of emissions, we suspect that the real-time quantification accuracy was compromised by both the gas temperature and the lack of sensitivity in responding to rapidly fluctuating release rates. This finding highlights the importance of considering operating conditions when interpreting OGI-based methane measurements in field settings.

4.2. Accuracy and Precision

Figures 4 and 5 represent the classification outcomes of the model under two contrasting environmental conditions, cold weather (−7 °C) and warm weather (30 °C). The

charts display the proportional distribution of true negatives (TN), true positives (TP), false negatives (FN), and false positives (FP) relative to the total number of predictions. These visualizations enable a direct comparison of the model's predictive behavior across different temperature regimes.

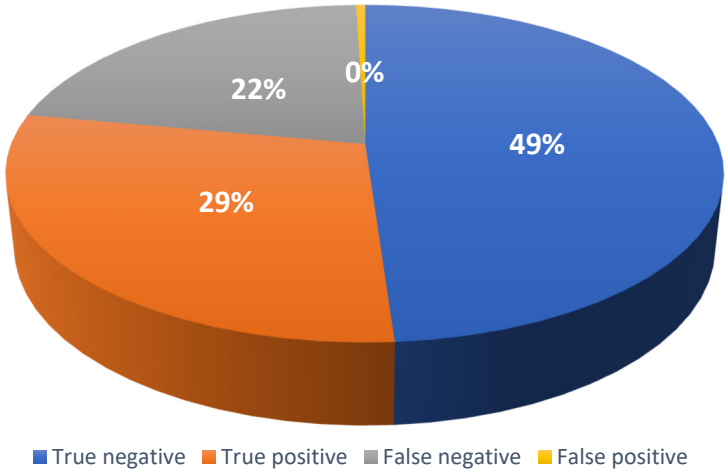


Figure 4. Detection percentages in cold weather.

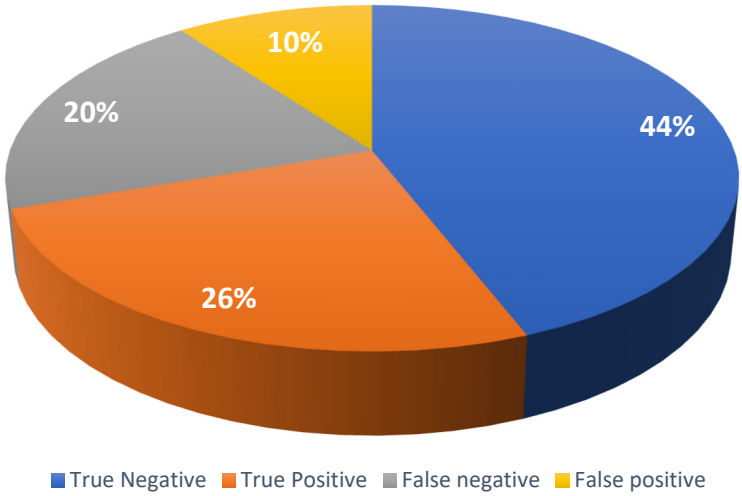


Figure 5. Detection percentages in warm weather.

Taken together, these two charts illustrate the extent to which environmental factors—particularly ambient temperature—can influence model reliability. In cold weather, the model prioritized specificity and precision by eliminating false positives, but at the expense of missing more true cases. In warm weather, the balance shifted: while the model slightly reduced false negatives, it did so by allowing a higher rate of false positives, thereby undermining both precision and accuracy. This trade-off underscores the need for adaptive calibration strategies, as the operational environment can significantly alter error patterns. From an application perspective, cold-weather performance may be advantageous in contexts where minimizing false alarms is critical, whereas warm-weather performance may be preferable in scenarios where maximizing detection is prioritized, even if it introduces additional false positives.

The performance of the classification model demonstrated clear dependence on environmental conditions, with a noticeable divergence between cold and warm weather scenarios. In cold weather, the model achieved an overall accuracy of 78% and a precision of 100%, with the outcome distribution consisting of 49% true negatives, 29% true positives,

22% false negatives, and 0% false positives. This outcome suggests that, under lower ambient temperatures, the system was highly reliable in avoiding false alarms, as every positive prediction corresponded to a true positive case. However, this conservative behavior came at the expense of sensitivity, as indicated by the relatively high false-negative rate (22%), meaning that nearly one-quarter of true-positive cases were not detected. Such a trade-off illustrates that the model, in cold conditions, is strongly biased toward specificity, favoring the correct classification of negative cases while overlooking a portion of actual positives. From a safety standpoint, the false negatives show a greater risk as they could not be seen and could therefore increase the global warming potential without us knowing.

In contrast, under warmer weather conditions (Figure 4), the model exhibited diminished overall performance, with accuracy decreasing to 70% and precision falling to 72.2%. The distribution of outcomes in this scenario shifted to 44% true negatives, 26% true positives, 20% false negatives, and 10% false positives. The reduction in precision was largely attributable to the increase in false positives, which rose from 0% in cold weather to 10% in warmer conditions. At the same time, the proportion of false negatives declined slightly from 22% to 20%, reflecting a modest gain in sensitivity. This suggests that, although the model was able to capture a slightly greater proportion of true positive cases in warmer environments, this improvement came at the cost of introducing a higher rate of incorrect alarms.

Finally, Figures 6 and 7 show methane plume detection and quantification with Optical Gas Imaging at two different ambient temperature conditions. In Figure 7, the OGI system quantified methane emissions at 1.4 kg/h and 1.6 kg/h from two distinct plumes within the field of view. The plumes are relatively diffused with less background contrast, demonstrating that elevated ambient temperatures reduce the thermal contrast between the surroundings and the gas plume. This reduction in thermal contrast worsens OGI sensitivity, resulting in reduced visibility of the plumes and an underestimation of the release rate compared to the actual controlled value.

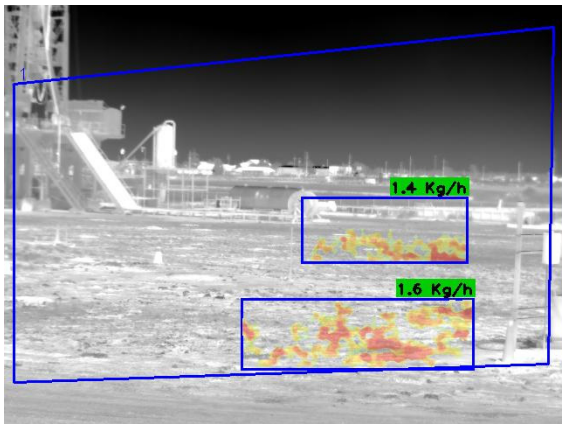


Figure 6. The gas plumes in a warm environment.

Additionally, visual clarity plays an essential role in plume detectability. On warmer days, brighter and more uniform backgrounds—such as sunlit skies or reflective surfaces—provided better visual contrast for the camera system. This reduced spectral interference from surrounding objects or materials, thereby minimizing background noise and improving plume visualization (see Figure 6). In contrast, colder days often featured dimmer lighting and mixed radiative backgrounds (e.g., cloudy skies, low sunlight angles), which can mask plumes or result in ambiguous detections (see Figure 7).

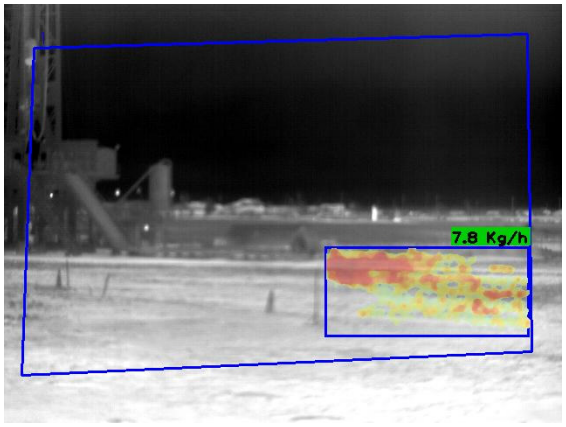


Figure 7. The gas plumes in a cold environment.

In contrast, Figure 7 contains a single plume of 7.8 kg/h. The plume is denser and has higher thermal contrast with the colder background in this case, enabling the OGI system to accurately capture the extent of the methane release. Improved sensitivity at low temperatures results in more accurate quantification, where the OGI-estimated rate is closer to the actual controlled release rate.

These findings explain the significant role of environmental factors, particularly temperature, in shaping model performance. Warmer weather may reduce the thermal contrast between targets and the surrounding background, introducing additional sensor noise and background interference that compromises class separability. From an application standpoint, this has critical implications. In operational contexts where false alarms are highly undesirable—such as when they trigger costly interventions or safety-critical responses—the cold-weather configuration is more advantageous due to its perfect precision. Conversely, in applications where the primary objective is to minimize the risk of missed detections, the warmer-weather condition provides a slight benefit by lowering the false negative rate; however, this advantage is counterbalanced by a reduction in overall reliability. These observations suggest that a single fixed decision threshold may not be adequate across varying environmental conditions. Instead, future work should consider temperature-adaptive calibration strategies, domain-specific threshold adjustment, or training data augmentation that explicitly accounts for seasonal and thermal variability. Such approaches would help mitigate the observed performance degradation and ensure consistent classification accuracy and precision across diverse operating environments.

5. Effect of Carbon Dioxide on Methane Detection

To investigate the influence of mixed-gas emissions on OGI performance, controlled experiments were conducted using a gas mixture consisting of two-thirds methane and one-third carbon dioxide. The mixture was released at a leak rate of 0.07–1.09 kg/h at a fixed distance of 45 m from the camera. Ambient temperature during the tests varied from 9 °C to 32 °C. Results are shown in Table 2. The camera was not trained to detect carbon dioxide. We wanted to check how CO_2 could interfere with methane and prevent or allow its detection.

Under these conditions, the OGI system was unable to detect any methane. No visible plume was observed in the infrared feed, and the Viper software failed to generate quantification values. Unlike tests conducted with pure methane, where detection probability increased with higher leak rates, the presence of CO_2 suppressed the infrared signal associated with methane. This resulted in an effective probability of detection (POD) of 0% across all tested leak rates.

Table 2. Comparison of OGI Methane Detection and Quantification for Pure Methane and Methane–CO_2 Mixtures.

Gas Composition	Leak Rate (kg/h)	Ambient Temperature (°C)	Detection Probability (%)	Quantification Success
CH_4 + CO_2 (2:1 ratio)	7.54 + 1.09	9	0	No
CH_4 + CO_2 (2:1 ratio)	22.7 + 0.65	16	0	No
CH_4 + CO_2 (2:1 ratio)	11.6 + 0.07	32	0	No

The most rational explanation for this masking effect lies in the infrared absorption characteristics of CO_2. Both CH_4 and CO_2 absorb in overlapping spectral bands, but CO_2 exhibits stronger absorption features in the wavelength region utilized by the OGI camera. As a result, the CO_2 fraction in the mixture attenuated or completely obscured the methane signal, preventing detection. In the case of complex gas mixtures, hyperspectral cameras can effectively distinguish methane from carbon dioxide by analyzing their unique spectral fingerprints. It can detect a wide range of narrow brands. Hyperspectral tools are more detailed and precise.

This finding has significant implications for field applications of OGI. In industrial settings, gas releases often consist of mixed compositions, particularly in processes involving combustion, flaring, or CO_2-rich natural gas. The inability of OGI to detect methane when CO_2 is present, even when methane is the dominant component, highlights a major limitation of current detection technologies. Without accounting for such masking effects, OGI surveys may substantially underreport methane emissions in environments where mixed-gas plumes are common.

6. Conclusions and Recommendations

This study investigates the impact of ambient temperature and gas composition on the performance of Optical Gas Imaging (OGI) technologies for methane leak detection and quantification, with a focus on understanding how environmental and mixture conditions affect both detectability and measurement accuracy.

The results show that ambient temperature plays a dual role in OGI performance. Higher temperatures increase the probability of detecting high-rate methane leaks, likely due to enhanced thermal contrast between the plume and the background. In contrast, lower temperatures improve the accuracy of leak quantification, suggesting more stable radiative conditions for estimating gas concentration. However, at −7 °C, the high incidence of false positives prevented the construction of reliable detection probability curves, indicating that very low temperatures can significantly compromise detection reliability. In addition, gas composition was found to strongly influence performance: the presence of carbon dioxide in a 2:1 methane–CO_2 mixture completely masked methane signals, preventing both detection and quantification. This effect is attributed to spectral overlap between methane and CO_2 in the infrared range, which reduces the sensor's ability to distinguish methane-specific absorption features.

These findings have important implications for field applications. Survey planning should account for environmental conditions: warmer temperatures are preferable for detection-focused surveys, while colder conditions are better for quantification. In mixed-gas environments where CO_2 or other interfering gases are present, OGI alone may be insufficient, and complementary methods such as extractive sampling, laser-based spectroscopy, or multi-gas sensors could be employed to compare the outcome. Careful calibration of OGI equipment for the expected gas composition and environmental conditions is essential, and operators must be trained to recognize false positives and adjust detection strategies accordingly. Finally, future research should investigate the threshold concentrations of

interfering gases that impair methane detection and explore OGI systems with broader spectral sensitivity or multi-gas capabilities to mitigate masking effects.

This study provides new insights into the combined effects of temperature and CO_2 interference on methane detection using Optical Gas Imaging, highlighting limitations that are not addressed in existing literature. The findings contribute to improving the reliability of OGI-based methane quantification under realistic environmental conditions.

Despite these findings, this study has several limitations. The analysis was conducted under controlled conditions that may not fully capture the variability of real-world environments, such as fluctuating atmospheric conditions, complex backgrounds, and dynamic plume dispersion. Furthermore, the results are specific to the OGI system and spectral range used, which may limit their generalizability to other sensors or configurations.

Furthermore, uncooled cameras are less sensitive compared to cooled cameras because they use uncooled sensors. For example, in warmer weather, we suspect better quantification would be achieved if a cooled camera were used. The only inconvenience found was that cooled cameras are more expensive than uncooled ones.

Author Contributions: Conceptualization, A.K.; methodology, A.K.; software, A.K.; validation, A.K. and H.E.; formal analysis, A.K.; investigation, A.K.; resources, A.K. and J.W.F.; data curation, A.K.; writing—original draft preparation, A.K.; writing—review and editing, A.K., J.W.F. and H.E.; visualization, A.K.; supervision, H.E.; project administration, H.E.; funding acquisition, H.E. All authors have read and agreed to the published version of the manuscript.

Funding: This research was funded by SLB grant number A22-0199-002.

Data Availability Statement: Dataset available on request from the authors.

Acknowledgments: We thank the Oil and Gas company SLB that provided the required OGI tool.

Conflicts of Interest: The authors declare no conflict of interest.

Nomenclature

Symbol	Description	Unit
MIR	Mid-infrared	μm
FIR	Far-infrared	μm
I	Initial Intensity of light	$W{\cdot}m^{-2}$
I_0	Intensity of light after travelling a distance	$W{\cdot}m^{-2}$
d	Distance	m
μ	Napierian absorption coefficient	m^{-1}
f	The bond force constant	Nm^{-1}
M_1	The mass of the atom 1	Kg
M_2	The mass of the atom 2	Kg
p	Predicted probability of detection	%
x	Input value (Methane flow rate)	Kg/hr
e	Euler's number	
β_0	Intercept term	
B_1	Coefficient for the input x	
TP	True positive	
TN	True negative	
FP	False positive	
FN	False negative	
T_p	Temperature of the gas plume	°C
T_s	Ambient background temperature	°C
ϵ_s	Emissivity of the background surface	
B(T)	Planck function	$w{\cdot}m^{-2}{\cdot}sr^{-1}{\cdot}m^{-1}$
Sr^{-1}	Per steradian (solid angle)	

References

1. Karakurt, I.; Aydin, G.; Aydiner, K. Sources and mitigation of methane emissions by sectors: A critical review. *Renew. Energy* **2012**, *39*, 40–48. [CrossRef]
2. Yusuf, R.O.; Noor, Z.Z.; Abba, A.H.; Hassan, M.A.A.; Din, M.F.M. Methane emission by sectors: A comprehensive review of emission sources and mitigation methods. *Renew. Sustain. Energy Rev.* **2012**, *16*, 5059–5070. [CrossRef]
3. THE GLOBAL METHANE CYCLE. Available online: https://articles.adsabs.harvard.edu/cgi-bin/nph-iarticle_query?bibcode=1993AREPS..21..407W&db_key=AST&page_ind=0&data_type=GIF&type=SCREEN_VIEW&classic=YES (accessed on 14 January 2025).
4. Climate Change 2021: The Physical Science Basis. Available online: https://www.ipcc.ch/report/ar6/wg1/ (accessed on 14 January 2025).
5. Souza Debossam, J.G.; de Souza, G.; Amaral Souto, H.P.; Pires, A.P. Numerical simulation of single-phase two-component non-Darcy flow in naturally fractured reservoirs for enhanced gas recovery and carbon dioxide storage. *Braz. J. Chem. Eng.* **2024**, *41*, 197–219. [CrossRef]
6. Emmanuel, O.; Ezeji, T.C. Advances in carbon dioxide capture and conversion technologies: Industrial integration for sustainable chemical production. *Next Sustain.* **2025**, *6*, 100108. [CrossRef]
7. Kebir, A.; Emadi, H.; Eyinla, D.; Navaid, H.B. Methane Detection using Optical Gas Imaging: Passive Infrared Technology. *J. Energy Technol. Policy* **2024**, *14*, 65–87. [CrossRef]
8. Shindell, D.; Bréon, F.M.; Collins, W.; Fuglestvedt, J.; Huang, J.; Koch, D. Anthropogenic and Natural Radiative Forcing. In *Climate Change 2013: The Physical Science Basis; Contribution of Working Group I*; Cambridge University Press: Cambridge, UK, 2013.
9. 1-12 Global Energy Balance n.d. Available online: https://www.meteor.iastate.edu/gccourse/forcing/spectrum.html (accessed on 4 March 2025).
10. IPCC. *Global Warming of 1.5 °C*; Cambridge University Press: Cambridge, UK, 2022. [CrossRef]
11. Energy Systems. *Climate Change 2022 Mitigation of Climate Change*; Cambridge University Press: Cambridge, UK, 2023; pp. 613–746. [CrossRef]
12. Navarro; Edmonds, J.; Faaij, A.; Edgar, H.; Damon, H.; David, I. *Mitigation of Climate Change*; Cambridge University Press: Cambridge, UK, 2014.
13. Zimmerle, D.; Vaughn, T.; Bell, C.; Bennett, K.; Deshmukh, P.; Thoma, E. Detection Limits of Optical Gas Imaging for Natural Gas Leak Detection in Realistic Controlled Conditions. *Environ. Sci. Technol.* **2020**, *54*, 11506–11514. [CrossRef]
14. Ravikumar, A.P.; Wang, J.; Brandt, A.R. Are Optical Gas Imaging Technologies Effective for Methane Leak Detection? *Environ. Sci. Technol.* **2017**, *51*, 718–724. [CrossRef] [PubMed]
15. Cui, F.X.; Zhao, Y.; Wang, A.J.; Ma, F.X.; Wu, J.; Li, Y.Y.; Dong, W.C. A Multi-Spectral Thermal Gas Detection Imager Using Uncooled Infrared Camera. *Optics* **2022**, *3*, 473–482. [CrossRef]
16. Ilonze, C.; Wang, J.; Ravikumar, A.P.; Zimmerle, D. Methane Quantification Performance of the Quantitative Optical Gas Imaging (QOGI) System Using Single-Blind Controlled Release Assessment. *Sensors* **2024**, *24*, 4044. [CrossRef] [PubMed]
17. Zimmerle, D.J.; Williams, L.L.; Vaughn, T.L.; Quinn, C.; Subramanian, R.; Duggan, G.P.; Robinson, A.L. Methane Emissions from the Natural Gas Transmission and Storage System in the United States. *Environ. Sci. Technol.* **2015**, *49*, 9374–9383. [CrossRef]
18. Smith, S.J.; Chateau, J.; Dorheim, K.; Drouet, L.; Durand-Lasserve, O.; Fricko, O.; Wada, K. Impact of methane and black carbon mitigation on forcing and temperature: A multi-model scenario analysis. *Clim. Change* **2020**, *163*, 1427–1442. [CrossRef]
19. Bell, C.; Rutherford, J.; Brandt, A.; Sherwin, E.; Vaughn, T.; Zimmerle, D. Single-blind determination of methane detection limits and quantification accuracy using aircraft-based LiDAR. *Elementa* **2022**, *10*, 186–188. [CrossRef]
20. Conrad, B.M.; Tyner, D.R.; Johnson, M.R. Robust probabilities of detection and quantification uncertainty for aerial methane detection: Examples for three airborne technologies. *Remote Sens. Environ.* **2023**, *288*, 113499. [CrossRef]
21. Weller, Z.D.; Roscioli, J.R.; Daube, W.C.; Lamb, B.K.; Ferrara, T.W.; Brewer, P.E.; von Fischer, J.C. Vehicle-Based Methane Surveys for Finding Natural Gas Leaks and Estimating Their Size: Validation and Uncertainty. *Environ. Sci. Technol.* **2018**, *52*, 11922–11930. [CrossRef]
22. Laitamäki, J. Comparing Properties of Different Infrared Cameras. Master's Thesis, Tampere University, Tampere, Finland, 2019.
23. Yilmaz, A. Radiation Transport Measurements in Methanol Pool Fires with Fourier Transform Infrared Spectroscopy NIST GCR09-922. Available online: https://www.nist.gov/publications/radiation-transport-measurements-methanol-pool-fires-fourier-transform-infrared (accessed on 20 February 2016).
24. Kwaśny, M.; Bombalska, A. Optical Methods of Methane Detection. *Sensors* **2023**, *23*, 2834. [CrossRef] [PubMed] [PubMed Central]
25. Safitri, A.; Mannan, M.S. Methane gas visualization using infrared imaging system and evaluation of temperature dependence of methane gas emissivity. *Ind. Eng. Chem. Res.* **2010**, *49*, 3926–3935. [CrossRef]
26. Riris, H.; Numata, K.; Li, S.; Wu, S.; Sun, X.; Abshire, J. LIDAR technology for measuring trace gases on Mars and Earth. *Atmos. Meas. Tech. Discuss.* **2010**, *3*, 4675–4705. [CrossRef]

27. Dong, L.; Li, C.; Sanchez, N.P.; Gluszek, A.K.; Griffin, R.J.; Tittel, F.K. Compact CH4 sensor system based on a continuous-wave, low power consumption, room temperature interband cascade laser. *Appl. Phys. Lett.* **2016**, *108*, 011106. [CrossRef]
28. Leupolt, A. Absorption of Methane in the Wavelength Region Around 3.3 μm: Laboratory Measurements and Comparison with Theoretical Computations. *Infrared Phys.* **1976**, *16*, 523–530. [CrossRef]
29. El-Azazy, M.; El-Shafie, A.S.; Al-Saad, K. Introductory Chapter: Infrared Spectroscopy—Principles and Applications. In *Infrared Spectroscopy—Perspectives and Applications*; IntechOpen: London, UK, 2023. [CrossRef]
30. Gilbert, A.S. IR Spectral Group Frequencies of Organic Compounds. *Encycl. Spectrosc. Spectrom.* **2017**, 408–418. [CrossRef]
31. Mayerhöfer, T.G.; Pahlow, S.; Popp, J. The Bouguer-Beer-Lambert Law: Shining Light on the Obscure. *Chemphyschem* **2020**, *21*, 2029–2046. [CrossRef] [PubMed]
32. McQuarrie, D.A.; Simon, J.D. *Physical Chemistry: A Molecular Approach*; The MIT Press: Cambridge, MA, USA, 1997.
33. Silva-Perez, C.; Marino, A.; Cameron, I. Monitoring agricultural fields using Sentinel-1 and temperature data in Peru: Case study of asparagus (*Asparagus officinalis* L.). *Remote Sens.* **2020**, *12*, 1993. [CrossRef]
34. Siddiqui, S.I.; Dong, H. Effects of Water Column Variations on Sound Propagation and Underwater Acoustic Communications. *Sensors* **2019**, *19*, 2105. [CrossRef] [PubMed]
35. Liu, L.; Sankarasubramanian, A.; Ranjithan, S.R. Logistic regression analysis to estimate contaminant sources in water distribution systems. *J. Hydroinformatics* **2011**, *13*, 545–557. [CrossRef]
36. Stoltzfus, J.C. Logistic regression: A brief primer. *Acad. Emerg. Med.* **2011**, *18*, 1099–1104. [CrossRef] [PubMed]
37. Sperandei, S. Understanding logistic regression analysis. *Biochem. Medica* **2014**, *24*, 12–18. [CrossRef]
38. LaValley, M.P. Logistic regression. *Circulation* **2008**, *117*, 2395–2399. [CrossRef]
39. Machine Learning for Methane Detection and Quantification from Space—A Survey n.d. Available online: https://www.researchgate.net/publication/383460781_Machine_Learning_for_Methane_Detection_and_Quantification_from_Space_%E2%80%94_A_survey (accessed on 11 March 2025).

Disclaimer/Publisher's Note: The statements, opinions and data contained in all publications are solely those of the individual author(s) and contributor(s) and not of MDPI and/or the editor(s). MDPI and/or the editor(s) disclaim responsibility for any injury to people or property resulting from any ideas, methods, instructions or products referred to in the content.